electronic reprint

STRUCTURAL SCIENCE
CRYSTAL ENGINEERING
MATERIALS

ISSN: 2052-5206
journals.iucr.org/b

A crystallographic excursion in the extraordinary world of minerals: the case of Cu- and Ag-rich sulfosalts

Luca Bindi and Cristian Biagioni

Acta Cryst. (2018). B**74**, 527–538

STRUCTURAL SCIENCE
CRYSTAL ENGINEERING
MATERIALS

ISSN 2052-5206

A crystallographic excursion in the extraordinary world of minerals: the case of Cu- and Ag-rich sulfosalts

Luca Bindi[a,b]* and Cristian Biagioni[c]

[a]Dipartimento di Scienze della Terra, Università di Firenze, Via La Pira 4, Firenze I-50121, Italy, [b]C.N.R., Istituto di Geoscienze e Georisorse, sezione di Firenze, Via La Pira 4, Firenze I-50121, Italy, and [c]Dipartimento di Scienze della Terra, Università di Pisa, Via S. Maria 53, Pisa I-56126, Italy. *Correspondence e-mail: luca.bindi@unifi.it

Received 29 July 2018
Accepted 13 October 2018

Edited by J. Lipkowski, Polish Academy of Sciences, Poland

Keywords: copper; silver; sulfosalts; crystal structure; ionic conductivity; minerals.

Copper and silver are common constituents in natural sulfosalts and can be present as minor or major components. Owing to the different kinds of coordination they can assume, these elements give rise to a number of sulfosalts that are usually quite complex to describe from a structural point of view because of the presence of twinning, disorder, polytypism and sometimes incommensurate modulation. Moreover, it is common to find them in different, partially occupied split sites, favoring the presence of strong ionic conductivity that can be related to a number of interesting technological properties. In this regard, a series of Cu- and Ag-rich sulfosalts showing an excess of these cations with respect to As, Sb and Bi is particularly interesting. Their crystal structures as well as their potential interest for materials science and solid-state physics are outlined. Copper- and mixed (Cu, Ag)-sulfosalts belonging to the wittichenite, tetrahedrite, galkhaite, routhierite and nowackiite series are discussed, together with some related compounds. Whereas in the wittichenite series Cu has either a trigonal planar or tetrahedral coordination, in members of the other series this element forms three-dimensional tetrahedral frameworks giving rise to cavities hosting other cations and anions. More difficult is the description of Ag-rich sulfosalts owing to the highly variable coordination environments shown by this element. Structural features of selected Ag sulfosalts together with members of the argyrodite series are discussed, highlighting the particular properties derived from the behavior of Ag.

1. Introduction

In 'sulfosalts' (or 'thiosalts'), a term firstly introduced by chemists in the XIXth century by analogy with complex salts of oxygen ('oxysalts'), we observe the combination of a simple cation with a complex anion $(MeS_m)^{n-}$, with S playing the same role of oxygen in oxysalts (Moëlo *et al.*, 2008). In this category of minerals, the transition elements copper (Z = 29) and silver (Z = 47) frequently occur either as minor or major components. These two elements occur as major components in several binary and ternary sulfosalts, for example, the Ag-bearing isotypes of the matildite series or the Cu sulfosalts belonging to the bournonite isotypic series. In addition, they can be minor components in several lead sulfosalts, for example, in the lillianite homeotypic series, $Ag_xPb_{3-2x}Bi_{2+x}S_6$ (Makovicky & Topa, 2014) or in some members of the sartorite homologous series (*e.g.* argentobaumhauerite; Topa & Makovicky, 2016). Note that these minor components can play important structural roles, being essential for the stabilization of complex sulfosalts [*e.g.* pellouxite, $(Cu,Ag)_2Pb_{21}Sb_{23}S_{55}ClO$; Palvadeau *et al.*, 2004]. In other cases, their ordering can give rise to incommensurate modulations,

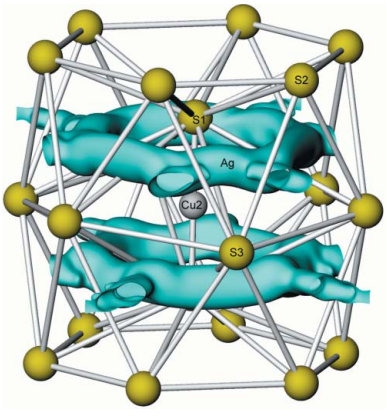

as in meneghinite (Bindi *et al.*, 2017*b*). Finally, Cu and Ag can be minor components without any essential structural role (*e.g.* Cu in zinkenite; Biagioni *et al.*, 2018).

In sulfosalts, Cu assumes a trigonal planar or tetrahedral coordination (rarely linear), whereas the coordination environment of Ag can range from linear to octahedral. In addition, they are frequently found in different, but very closely adjacent sites, favoring the presence of strong ionic conductivity. A series of Cu- and Ag-rich sulfosalts show an excess of these small formally monovalent cations with respect to As, Sb and Bi. In some cases, extensive Cu-for-Ag substitution can be observed (*e.g.* in the tetrahedrite isotypic series), whereas in other cases one element can be, to the best of our knowledge, only partially substituted by the other (*e.g.* in the nowackiite isotypic series or in the pyrargyrite–proustite pair). Several of these species have gained increasing interest in material sciences owing to their several potential technological applications (*e.g.* photoelectric and thermoelectric properties, ion conductivity). In this respect, the structural investigation of natural Cu- and Ag-rich sulfosalts may be extremely important and can help in orienting the synthesis of specific compounds and in understanding their crystal structures. Indeed, natural materials are often well crystallized because of the prolonged annealing times, and their crystallization occurs in physico–chemical complex environments, producing compounds which have a very rich and variable crystal chemistry that can provide valuable information and address the synthesis works in a very profitable way. Consequently, in this review, the main series of Cu- and Ag-rich sulfosalts is discussed, following the classification by Moëlo *et al.* (2008). Unclassified Cu sulfosalts with undetermined crystal structures have not been taken into account. In contrast, the argyrodite–canfieldite series, though not belonging to the sulfosalt realm *sensu stricto* (s.s.) has been discussed owing to its affinity with other Ag sulfosalts and its interesting technological properties.

2. The Cu- and mixed (Cu, Ag)-rich sulfosalts

2.1. Wittichenite series

The wittichenite homeotypic series comprises three mineral species (Fig. 1): wittichenite, Cu_3BiS_3; skinnerite, Cu_3SbS_3; and the recently described species bytízite, Cu_3SbSe_3. These phases are emerging semiconductors and potential candidates for photovoltaics, showing suitable optical properties for solar cells (*e.g.* Kehoe *et al.*, 2013; Yan *et al.*, 2013).

The crystal structure of wittichenite (Fig. 1*a*) was solved by Matzat (1972) and Kocman & Nuffield (1973) in the space group $P2_12_12_1$, with unit-cell parameters $a = 7.72$, $b = 10.40$ and $c = 6.72$ Å. Copper is in a distorted planar triangular coordination and Bi is at the vertex of a trigonal pyramid.

The crystal structure of wittichenite is isotypic with the low-temperature polymorph of Cu_3SbS_3 and it remains stable up to 227°C (Wei *et al.*, 2018). Indeed, this compound shows an interesting case of temperature-dependent polymorphism (*e.g.* Makovicky, 1994; Pfitzner, 1994). At $T < -10$°C, Cu_3SbS_3 is orthorhombic (space group $P2_12_12_1$ and unit-cell parameters $a = 7.84$, $b = 10.22$, $c = 6.60$ Å; Whitfield, 1980). In its crystal structure, all Cu atoms are in a trigonal planar coordination. Between −10 and 122°C, the monoclinic pseudo-orthorhombic polymorph, known as skinnerite, occurs. Its crystal structure (Fig. 1*b*) was investigated through Rietveld refinement by Makovicky & Balić-Žunić (1995) and Pfitzner (1998) using synthetic Cu_3SbS_3. The space group symmetry of skinnerite is $P2_1/c$, with unit-cell parameters $a = 7.81$, $b = 10.24$, $c = 13.27$ Å and $\beta = 90.3°$ (Makovicky & Balić-Žunić, 1995). Antimony has the typical trigonal pyramidal coordination of all the members of the series. Most of the Cu sites display a trigonal planar coordination, whereas one Cu site is split into two distorted tetrahedral [3 + 1] polyhedra. Crystals of skinnerite are intimately twinned, owing to the transition between the high-temperature ion-conducting polymorph of *Pnma* Cu_3SbS_3 and low-temperature $P2_1/c$ skinnerite.

The orthorhombic high-temperature phase is stable above 122°C and was studied in detail by Skinner *et al.* (1972). Pfitzner (1998) determined the crystal structure of the high-temperature Cu_3SbS_3 at 220° and 130°C in the space group *Pnma*, with unit-cell parameters $a = 7.81$, $b = 10.25$ and $c = 6.59$ Å. Copper atoms are disordered among the three-dimensional arrangement of SbS_3 groups. The atomic displacement parameters of these disordered Cu atoms was modeled using a Gram–Charlier non-harmonic approach, deriving a suggestion for a pathway for mobile Cu atoms. Copper is distributed over five independent trigonal or tetrahedral positions.

In these compounds, short Cu–Cu distances ranging from 2.6 to 2.9 Å occur. In wittichenite, spirals of short Cu–Cu distances parallel to [001] occur; in skinnerite, these spirals are

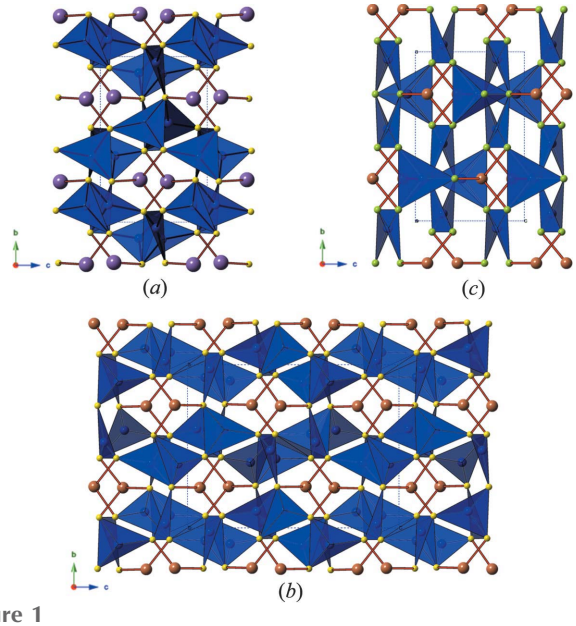

Figure 1
Crystal structures of members of the wittichenite series as seen down [100]: (*a*) wittichenite, (*b*) skinnerite and (*c*) bytízite. Symbols: blue polyhedra = Cu sites. Circles: green = Se; light brown = Sb; violet = Bi; yellow = S. For clarity, only one split tetrahedral position is shown.

replaced by finite chain fragments (Makovicky & Balić-Žunić, 1995).

The crystal structures of Cu_3SbS_3 and Cu_3BiS_3 are considered as examples of endopolytypism. Their crystal structures can be formed by stacking wavy unit layers (001) of Cu atoms distributed in two different ways within an unchanging (Sb,Bi)–S framework (Makovicky, 1994).

At room temperature, the *Pnma* structure is also shown by Cu_3SbSe_3 (Fig. 1*c*), as described by Whitfield (1980) and Pfitzner (1995). Recently, Škácha *et al.* (2018) described this compound as the new mineral bytízite, the orthorhombic Se homeotype of skinnerite, with unit-cell parameters a = 7.96, b = 10.58 and c = 6.82 Å.

2.2. The tetrahedrite isotypic series

The tetrahedrite isotypic series is possibly one of the most complex groups of sulfosalts and it is actively studied both for its geological and economic significance (*e.g.* George *et al.*, 2017) as well as for its technological applications, *e.g.* thermoelectric properties (Lu & Morelli, 2013; Suekuni *et al.*, 2013; Chetty *et al.*, 2015).

First solved by Machatschki (1928*a*,*b*), who proposed the ideal composition Cu_3SbS_3, the crystal structure of tetrahedrite was modeled by Pauling & Neuman (1934) as a derivative of the sphalerite structure and assuming a stoichiometry of $Cu_{12}Sb_4S_{13}$, which was in closer agreement with available chemical data. The first detailed description of the structural arrangement of tetrahedrite was given by Wuensch (1964). Since then, several structural refinements, both on natural and synthetic samples, have been reported (*e.g.* Wuensch *et al.*, 1966; Kalbskopf, 1972, 1974; Makovicky & Skinner, 1979; Johnson & Burnham, 1985; Peterson & Miller, 1986; Dmitrieva *et al.*, 1987; Rozhdestvenskaya *et al.*, 1993; Pfitzner *et al.*, 1997; Foit & Hughes, 2004; Makovicky *et al.*, 2005; Andreasen *et al.*, 2008; Pervukhina *et al.*, 2010*b*; Nasonova *et al.*, 2016; Škácha *et al.*, 2016).

Tetrahedrite is cubic, with space group $I\bar{4}3m$. It can be considered as a derivative of the sphalerite structure with extensive omission, substitution and insertion of new sites. Three cation and two anion sites occur in its crystal structure (Fig. 2). Cations are hosted at the M(1), M(2) and X sites, at the Wyckoff positions 12*d*, 12*e* and 8*c*, respectively; anions occur at the Y and Z sites, at Wyckoff positions 24*g* and 2*a*, respectively. M(1) is tetrahedrally coordinated by four Y anions, whereas M(2) has a trigonal planar coordination, being bonded with one Z and two Y anions. According to some authors (*e.g.* Andreasen *et al.*, 2008), the M(2) is a split flat pyramidal site, statistically located on both sides of the Y–Y–Z coordination triangle at Wyckoff position 24*g*. M(1) and M(2) sites are able to host several cations, such as Cu^+, Ag^+, Zn^{2+}, Fe^{2+}, Hg^{2+}, Cd^{2+}, Mn^{2+}, Cu^{2+} and Fe^{3+}. In some cases, vacancies are present (*e.g.* in goldfieldite – Pohl *et al.*, 1996). Natural samples usually show ten (Cu + Ag) atoms per formula unit (apfu) and two (Fe, Zn, Hg . . .) apfu (*e.g.* Johnson *et al.*, 1986), the latter distributed over the tetrahedral M(1) site. These types of tetrahedrites are usually reported as 'fully substituted'. However, 'unsubstituted' [*i.e.* tetrahedrites having 12 (Cu + Ag) apfu] or 'not-quite-fully substituted' samples are known (*e.g.* Makovicky *et al.*, 2005). The X site hosts Sb^{3+}, As^{3+}, Bi^{3+} and Te^{4+} in trigonal pyramidal coordination. The Y site is tetrahedrally coordinated by two M(1), one M(2) and one X site, whereas six M(2) sites are bonded to the Z site. The Y and Z sites could host S and Se; in some samples, the Z site was found to be vacant (*e.g.* Rozhdestvenskaya *et al.*, 1993).

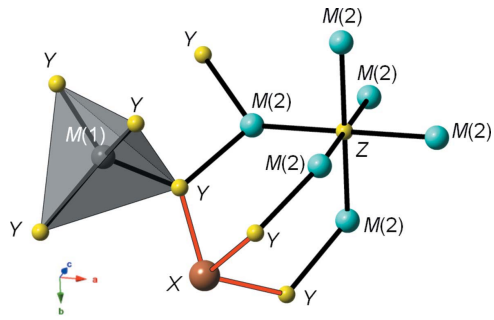

Figure 2
Arrangement of cation and anion sites in the crystal structure of the members of the tetrahedrite isotypic series.

The structural formula of the members of the tetrahedrite isotypic series can be written as $M(2)_6M(1)_6X_4Y_{12}Z$ (Z = 2). Several homovalent and heterovalent substitutions involving the different sites of the tetrahedrite structure give rise to eleven known mineral species as well as a large number of synthetic analogs. The structural flexibility allows the accommodation of several cations of medium-to-small atomic radius and variable formal charges (from +1 to +4), as well as the occurrence of vacancies or interstitial atoms (*e.g.* Maske & Skinner, 1971; Makovicky & Skinner, 1979; Makovicky *et al.*, 2005). This variability encompasses anions too, with the substitution of S by Se or with the occurrence of vacancies at the Z site. Owing to this wide range of possible chemical substitutions, tetrahedrite has been referred to as a 'sulfide amphibole' (Sack & Loucks, 1985).

Johnson *et al.* (1988) stressed that tetrahedrite (and its isotypes) is an example of a sulfidic sodalite-like (SOD) highly collapsed framework, with cavities that can be described as Laves polyhedra, *i.e.* truncated tetrahedra. This relationship between tetrahedrite and sodalite was first referenced by Belov & Pobedimskaya (1969), even though the original insight was attributed to Pauling, who solved the crystal structures of sodalite and tetrahedrite (Pauling, 1930; Pauling & Neuman, 1934). However, no mention of this relationship can be found in either of the two papers by Pauling (*e.g.* Nyman & Hyde, 1981). The stoichiometric relationship with sodalite becomes obvious by rearranging the chemical formula to yield $|M(2)_{12}X_8Z_2|[M(1)_{12}Y_{24}]$. Indeed, tetrahedrite is made up of a sodalite-like framework of corner-connected $M(1)Y_4$ tetrahedra with cages containing Z-centered $M(2)_6$-octahedra (Fig. 3*a*), encircled by four XY_3 trigonal pyramids (*e.g.* Johnson *et al.*, 1988).

The wide chemical variability of tetrahedrite isotypes prompted several structural and spectroscopic investigations involving either natural and synthetic tetrahedrites in order to

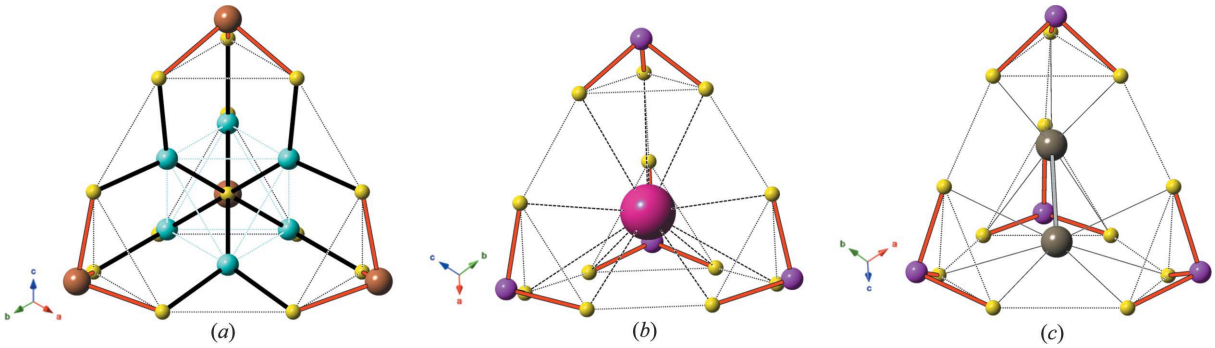

Figure 3
The Laves polyhedron in the isotypic series of (*a*) tetrahedrite, (*b*) galkhaite and (*c*) routhierite. Circles: gray = Tl; light blue = Cu/Ag; light brown = Sb; magenta = As; violet = Cs; yellow = S.

understand the role of certain components such as Fe (*e.g.* Makovicky *et al.*, 1990, 2003; Nasonova *et al.*, 2016), Hg (*e.g.* Foit & Hughes, 2004), Te and Se (*e.g.* Karup-Møller & Makovicky, 1999; Makovicky & Karup-Møller, 2017) Co, Ni, Mn, Sn, Ge, Pb, Ga and In [Makovicky (2006) and references therein], as well as Ag (*e.g.* Pattrick & Hall, 1983). In particular, it has been shown that Ag preferentially occupies the threefold coordinated 12*e* *M*(2) site (Kalbskopf, 1972; Johnson & Burnham, 1985; Peterson & Miller, 1986). High-silver tetrahedrites display an unusual behavior: as the Ag content increases, the unit cell edge initially increases and then it tends to decrease. Rozhdestvenskaya *et al.* (1993) interpreted this unusual behavior as related to the vacancy at the *Z* position and the formation of an octahedral Ag cluster around this position, with Ag–Ag distances similar to those observed in metallic Ag. Another feature shown by Ag-rich tetrahedrite is the high-temperature factor of the octahedrally coordinated *Z* site, correlating with the amount of Ag. This feature was explained by Peterson & Miller (1986) as the result of positional disorder caused by the longer Ag—S bonds displacing the S atoms. When averaged over many unit cells, such a displacement appears as increased thermal motion.

Makovicky *et al.* (2005) studied a Cu-excess tennantite, ideally $Cu_{12.5}As_4S_{13}$. The basic structural arrangement is the same as shown by other 'tetrahedrites'; the unique feature is represented by the occurrence of disordered Cu atoms located in two partially occupied Cu2 sites (Cu2*A* and Cu2*B*) only 1.08 Å from each other. It is likely that such disorder could have a dynamic nature. A similar situation of Cu disorder was previously reported by Makovicky & Skinner (1979). However, in the sample studied by these latter authors and having a chemical composition of $Cu_{13.8}Sb_4S_{13}$, the additional site was located close to the tetrahedral *M*(1) site.

2.3. Galkhaite and its isotypes vorontsovite and ferrovorontsovite

Galkhaite, ideally $Hg_5CuCsAs_4S_{12}$, is the only caesium sulfosalt known to date. A short review of the crystallographic studies performed on this mineral is given by Biagioni *et al.* (2014*a*). Galkhaite is cubic, and crystallizes in the space group $I\bar{4}3m$. One anion and three cation sites occur in its crystal structure. Cations are hosted at the Hg (Wyckoff position 12*d*), Cs (2*a*) and As (8*c*) sites; S is hosted at Wyckoff position 24*g*. The crystal structure is formed by a tetrahedrite-like framework, with $(Hg,Cu)S_4$ tetrahedra and $(As,Sb)S_3$ flat trigonal pyramids. Whereas in tetrahedrite the Laves polyhedra hosted a $ZM(2)_6$ polyhedra (Fig. 3*a*), in galkhaite these large 12-fold coordinated cavities host Cs (Fig. 3*b*). The chemical variability of galkhaite is related to the possible substitution of minor Hg by Zn and Fe, and Cu by Ag. Biagioni *et al.* (2014*a*) examined three different specimens and described the slight structural variations related to this chemical variability.

Makovicky (2005) stressed the porous nature of this sulfosalt and in this respect galkhaite could host other large cations, replacing Cs^+, such as Tl^+ and possibly NH_4^+. Recently, the thallium analog of galkhaite has been described from the Vorontsovskoe deposit, Urals Region, Russia, by Kasatkin *et al.* (2018) and named vorontsovite, ideally $Hg_5CuTlAs_4S_{12}$. The same authors described also the Fe isotype ferrovorontsovite, $Fe_5CuTlAs_4S_{12}$, from the same Russian locality.

2.4. The routhierite isotypic series

Routhierite, ideally $CuHg_2TlAs_2S_6$, is a very rare thallium sulfosalt first described from Jas Roux, Hautes-Alpes, France (Johan *et al.*, 1974). Graeser *et al.* (1995) described its Zn analog, stalderite, $CuZn_2TlAs_2S_6$, from Lengenbach, Switzerland, and solved its crystal structure. Recently this group of thallium sulfosalts has become broader following the discovery of new species from the Monte Arsiccio mine and the Lengenbach quarry: arsiccioite, $AgHg_2TlAs_2S_6$ (Biagioni *et al.*, 2014*d*), ralphcannonite, $AgZn_2TlAs_2S_6$ (Bindi *et al.*, 2015*a*) and ferrostalderite, $CuFe_2TlAs_2S_6$ (Biagioni *et al.*, 2016). Moreover, the crystal structure of routhierite has been solved (Bindi, 2008; Biagioni *et al.*, 2014*c*).

Members of this isotypic series crystallized in the space group $I\bar{4}2m$. Formally, monovalent (Cu, Ag) and divalent (Hg, Zn, Fe) metals are tetrahedrally coordinated by two independent S atoms (at Wyckoff positions 16*j* and 8*i*, respectively), and are hosted within two sites, *M*(1) (at 4*d*) and *M*(2) (at 8*f*). Bindi (2008) and Biagioni *et al.* (2014*c*) showed that in the crystal structure of routhierite, Cu is hosted at the smaller *M*(1) site, whereas *M*(2) hosts the larger Hg atom. The finding of the Ag isotype of routherite, arsiccioite (Biagioni *et al.*,

2014*d*), proved that an unexpected cation distribution occurs in Ag-rich 'routhierites'. Indeed, one should expect the simple homovalent substitution of Cu by Ag at the *M*(1) site. On the contrary, this site showed a mixed (Hg, Ag, Cu) occupancy, whereas Ag partially replaces Hg at the *M*(2) site. Consequently, the structural formula of arsiccioite should be correctly written as $^{M(1)}Hg^{M(2)}(Ag_{0.5}Hg_{0.5})_2TlAs_2S_6$. This result was later confirmed by Bindi *et al.* (2015*a*), who proposed the ideal structural formula $^{M(1)}Zn^{M(2)}(Ag_{0.5}Zn_{0.5})$-0.5)$TlAs_2S_6$ for ralphcannonite. Consequently, in routhierite isotypes, the size of cations has priority over the valence state in governing the metal distribution between tetrahedral *M*(1) and *M*(2) sites.

The tetrahedral sites are connected through corner-sharing, forming a three-dimensional framework with channels parallel to [001] containing TlS_6 and (As, Sb)S_3 polyhedra. Pairs of large Tl cations are hosted within cavities similar to Laves polyhedra (Fig. 3*c*). The Tl site has a very dissymmetric (2 + 4) coordination, possibly the result of strong stereochemical activity of the 6*s* lone pair of Tl^+. The Tl coordination can be described as an orthorhombic pyramid with a split apex; on the other side of the apex, a relatively short Tl–Tl distance (∼3.3 Å) occurs, probably indicating some type of Tl–Tl interaction. In some cases, the Tl site was found split (*e.g.* in arsiccioite; Biagioni *et al.*, 2014*d*).

2.5. Nowackiite isotypic series and related minerals

Three copper sulfosalts whose crystal structure can be described as a defect sphalerite structure, in which some S positions along the three axes remain empty, form the nowackiite isotypic series (Fig. 4*a*).

Nowackiite, $Cu_6Zn_3As_4S_{12}$, was described by Marumo & Burri (1965) from the Lengenbach quarry, Switzerland. Its crystal structure was solved by Marumo (1967) in the space group *R*3, with unit-cell parameters *a* = 13.44 and *c* = 9.17 Å. The *c* axis of nowackiite is parallel to the [111] direction of sphalerite. Copper and zinc are tetrahedrally coordinated in two independent sites, whereas As shows the typical trigonal pyramidal coordination. As noted by Marumo (1967), As–As distances are shorter than the normal (*i.e.* 3.4 Å).

Vasil'ev (1968) described aktashite, $Cu_6Hg_3As_4S_{12}$, from the Aktash Hg deposit, Gornyi Altai, Russia. Its crystal structure was solved by Kaplunnik *et al.* (1980) and refined by Vasil'ev *et al.* (2010) and Biagioni *et al.* (2014*b*). Nowacki (1982) pointed out the isotypysm between nowackiite and aktashite. The unit-cell parameters of the latter are larger, owing to the Zn–Hg substitution, *i.e.* *a* = 13.73, *c* = 9.33 Å.

The nowackiite series is completed by the Sb analog of aktashite, gruzdevite, $Cu_6Hg_3Sb_4S_{12}$, described by Spiridonov *et al.* (1981).

Following Krivovichev & Filatov (1999), Vasil'ev *et al.* (2010) described the crystal structure of aktashite using an anion-centered approach. All S atoms are tetrahedrally coordinated by cations and these S-centered tetrahedra form a three-dimensional framework hosting an empty $[As_4]^{12+}$ tetrahedron. The small cluster $[As_4S_{12}]^{12-}$ is the most interesting feature of the crystal structure of nowackiite and aktashite and has been studied by several authors (*e.g.* Gabuda *et al.*, 2009).

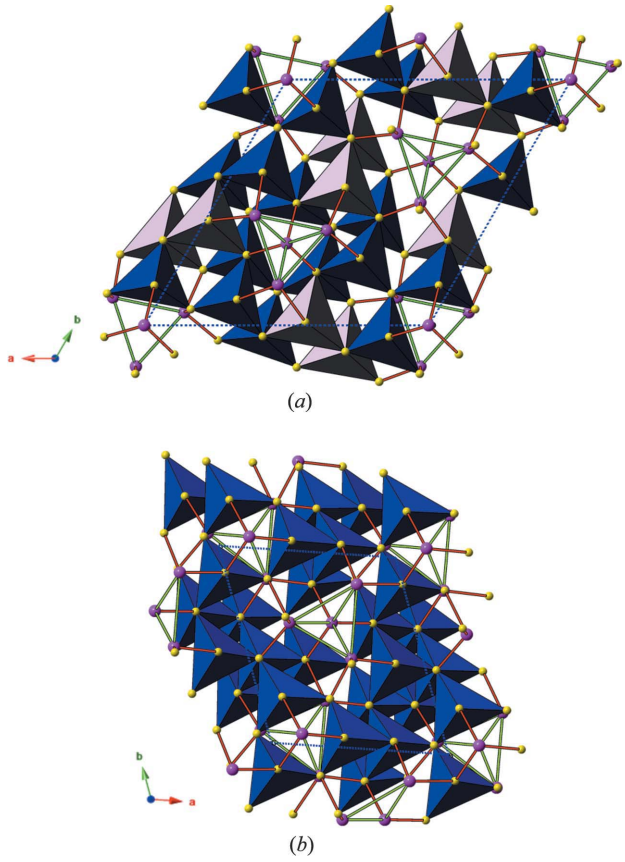

Figure 4
The tetrahedral framework of nowackiite isotypes [in (*a*) the crystal structure of aktashite is shown] and (*b*) sinnerite. Polyhedra represent Cu (blue) and Hg (gray) sites. Circles: magenta = As; yellow = S. The relatively short As–As distances are shown as thick green lines, in order to highlight the occurrence of As_4 clusters.

The same $[As_4S_{12}]$ clusters were observed in another mineral showing close relations with the sphalerite structure, *i.e.* sinnerite, $Cu_6As_4S_9$, first described from the Lengenbach quarry, Switzerland, by Marumo & Nowacki (1964). The relationship with the sphalerite structure was highlighted by Makovicky & Skinner (1972), who were able to determine the composition and symmetry of sinnerite using the synthetic material obtained by Maske & Skinner (1971). Makovicky & Skinner (1972) demonstrated that sinnerite is triclinic, and reported the widespread twinning by reticular pseudo-merohedry, characterizing both natural and synthetic material. A structural model was proposed by Makovicky & Skinner (1975) using a synthetic crystal. These authors showed that the twinning of $Cu_6As_4S_9$ gives rise to twin aggregates formed by 24 individuals and simulating a $\bar{4}3m$ symmetry. Later, Bindi *et al.* (2013*a*) solved the crystal structure using an untwinned crystal from Lengenbach. Sinnerite is triclinic, space group *P*1, with unit-cell parameters *a* = 9.10, *b* = 9.86, *c* = 9.11 Å and α = 90.3, β = 109.5, γ = 107.6°. A total of eight different AsS_3 trigonal pyramids and 12 independent CuS_4 tetrahedra occur in the crystal structure (Fig. 4*b*). Taking into account the

shortest (the strongest) As–S distances, two types of As_mS_n chains can be identified, with compositions As_3S_7 and As_5S_{11}. These chains are surrounded by CuS_4 tetrahedra. Two distinct groups of As_4S_{12} clusters can be identified, with As–As distances ranging from 3.36 to 3.62 Å.

Whereas the species so far described have a three-dimensional tetrahedral framework based on the sphalerite substructure, laffittite, $AgHgAsS_3$, has a similar framework based on the PbS archetype. First found by Johan *et al.* (1974) from Jas Roux, France, laffittite was reported from few other localities worldwide. Nakai & Appleman (1983) solved its crystal structure that was later refined by Pervukhina *et al.* (2010*a*) and Biagioni *et al.* (2014*b*). Laffittite is monoclinic, space group *Cc*, with unit-cell parameters (after Biagioni *et al.*, 2014*b*) a = 6.67, b = 11.33, c = 7.76 Å, β = 115.3°. Silver has a (3 + 1) coordination whereas Hg has a (2 + 2) tetrahedral coordination, with the two shorter distances in a linear arrangement. Arsenic forms the typical AsS_3 groups that are hosted within cavities of the Ag- and Hg-centered tetrahedral framework.

3. Ag-rich sulfosalts and related compounds

3.1. Samsonite and stephanite

Samsonite, $Ag_4MnSb_2S_6$, represents one of the few Mn-sulfosalts in the mineral kingdom. Its crystal structure was determined by Edenharter & Nowacki (1974) and later re-examined by Bindi & Evain (2007). The latter authors used this mineral as an example to show to the mineralogical community that the non-harmonic approach, based upon a Gram–Charlier development of the atomic displacement factors, can be useful in mineral sciences for the determination of still unknown structures. The same approach was then used by Leitl *et al.* (2009) to describe the crystal structure of stephanite, Ag_5SbS_4.

The non-harmonic approach (Johnson & Levy, 1974; Zucker & Schulz, 1982) can be easily explained with the use of higher order tensor elements in the expression of structure factors. Such a method gives an equivalent description, though with less parameters, than the split-atom model in the case of disorder with highly overlapping electron densities (Kuhs, 1992). This alternative approach, in particular the Gram–Charlier formalism, provides an easier convergence of the refinement due to much lower correlations between the refined parameters.

Bindi & Evain (2007) found that the Mn atoms form slightly deformed MnS_6 octahedra and the Sb atoms are in a threefold coordination occupying the top of a trigonal pyramid with three S atoms making the base. SbS_3 polyhedra are isolated from each other. The Ag atoms exhibit two different crystal-chemical environments: Ag1 is found to be tetrahedrally coordinated by four S atoms, whereas Ag2 is triangularly coordinated by three S atoms (Fig. 5*a*). This structure description of the atomic arrangement of samsonite at room temperature is very similar to that previously reported by Edenharter & Nowacki (1974). Nevertheless, Bindi & Evain (2007) studied in detail the size and the shape of the anisotropic displacement parameters because possible strong anisotropy could reflect static or dynamic disorder related to positional disorder or anharmonicity of the fine structure. They observed that the Ag atoms show strongly anisotropic displacement parameters well visible when the structure is projected along the *c* axis, and modeled it by means of a Gram–Charlier development of the anisotropic displacement factors.

To verify the structural model given by Ribár & Nowacki (1970) for stephanite and to possibly provide information on the diffusion pathways of silver in the structure, Leitl *et al.* (2009) applied the non-harmonic approach. Indeed, the crystal structure of stephanite (Fig. 5*b*) had been originally determined by Ribár & Nowacki (1970) in the space group $Cmc2_1$. Although their structural model was correct, Ribár & Nowacki reported an R value of 9.4% and B_{iso} values of 3.82, 4.49 and 3.33 $Å^2$ for the Ag1, Ag2 and Ag3 positions, respectively (approximately up to three times the values observed for Sb and for the S atoms).

Although Leitl *et al.* (2009) confirmed the main structural features previously reported, they also introduced new aspects. For example, one of the silver positions was refined by using non-harmonic parameters of the third order according to Gram–Charlier (Zucker & Schulz, 1982). A careful analysis of the pathways of silver diffusion in the crystal structure of stephanite showed that, in contrast to the pyrargyrite structure (Leitl, 2007; Bindi *et al.*, 2010), a connection exists between the Ag–Ag distances and the activation energy. Several short Ag–Ag distances range from 2.90 to 3.05 Å, a second group of metal distances is between 3.25 and 3.50 Å and a longer distance of more than 3.8 Å is present between Ag1 and Ag3. Along the latter direction, the highest activation energy of almost 1.0 eV is obtained, which is necessary for the silver atom to jump to the next noble metal site. After an analysis of the energy barriers between the silver sites, the preferred ion diffusion pathways within the crystal structure of stephanite were defined (Leitl *et al.*, 2009). The charge transport by Ag

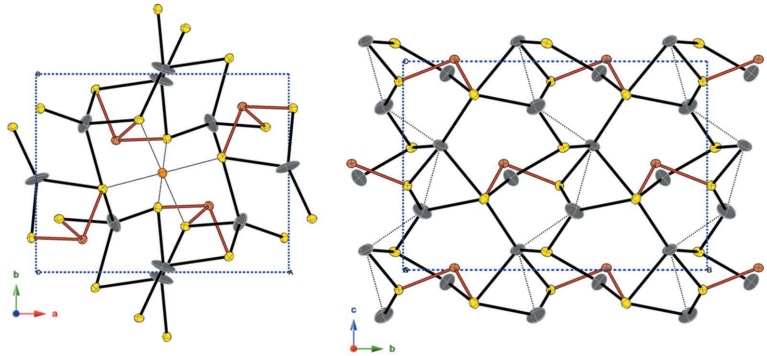

Figure 5
Crystal structures of (*a*) samsonite and (*b*) stephanite projected along [001] and [100], respectively. Atoms are shown using thermal ellipsoids. Ag—S and Sb—S bonds are shown as thick black and red lines, respectively. Short Ag–Ag contacts are drawn as dotted lines. Circles are Ag (dark gray), Sb (light brown) and S (yellow) sites.

ions happens preferably along pathways with low activation energies, which for stephanite are the routes along the sites Ag1 and Ag2 with distances of about 3.0 Å.

3.2. Proustite and pyrargyrite series

Proustite and pyrargyrite were officially recognized as new mineral species by Beudant (1832) and Glocker (1831), respectively, although Proust reported proustite as early as 1804. Crystallographic studies of Harker (1936), Hocart (1937), Engel & Nowacki (1966) and Laufek *et al.* (2010) show that proustite and pyrargyrite are trigonal and belong to space group *R*3*c*. It should be noted that xanthoconite and pyrostilpnite, the rare low-temperature polymorphs of proustite and pyrargyrite, respectively, are both monoclinic, and crystallize in the space group *C*2/*c* (*e.g.* Beland, 1948; Weil & Hocart, 1953; Hall, 1966; Lange *et al.*, 1993); in eckerite, $CuAg_2AsS_3$, one third of independent Ag positions are occupied by Cu (Bindi *et al.*, 2015*b*).

The crystal structure of proustite (Fig. 6) consists of two sets of spiral chains parallel to the *c* axis. Each chain is built of alternating Ag and S atoms, and the chains of each set are interconnected by As/Sb atoms, which are the apices of flat pyramidal AsS_3/SbS_3 groups. Each S atom is part of a different Ag—S chain. The Sb-for-As substitution tends to flatten still further the pyramidal groups, thereby increasing the separation of the chains from one another (Toulmin, 1963).

By means of a crystal-chemical study of 32 natural samples of proustite and 27 samples of pyrargyrite from different localities and variable chemical compositions, Bindi *et al.* (2010) were able to model the unit-cell parameters as a function of the Sb content. These authors found that the *a* parameter is strongly influenced by the As↔Sb substitution whereas the influence on the *c* parameter is very minor (nearly constant trend). The following equations to predict (subscript pred) the unit-cell values were obtained from the linear fitting of the data:

$$a_{\rm pred} = 10.8433\,(3) + 0.2019\,(4)\,{\rm Sb},$$

$$c_{\rm pred} = 8.7189\,(6) + 0.0059\,(9)\,{\rm Sb},$$

$$V_{\rm pred} = 887.77\,(7) + 34.0\,(1)\,{\rm Sb}.$$

The compositional data support the concept that proustite–pyrargyrite solid solutions re-equilibrate and exsolve to near end-member upon cooling. Indeed, examples of intermediate compositions are extremely rare in nature and, if any, must have quenched above the *solvus*.

At about 30°C (~10°C for pyrargyrite) proustite undergoes a second-order phase transition, exhibiting a positive nonsymmetry breaking spontaneous strain of the unit cell. This strain is provoked by the onset of thermally induced hopping of Ag ions, as revealed by impedance spectroscopy (Schönau & Redfern, 2002). At about 150°C, the high-frequency conductivity of proustite increases as a function of the increasing random disorder of Ag within possible unoccupied sites in the structure. When almost all Ag ions are disordered, a transition to fast ion conduction at ~270°C in proustite (and ~220°C in pyrargyrite) is observed. At high temperatures, Ag is maximally disordered, the structure itself is weakened and the mineral starts to decompose.

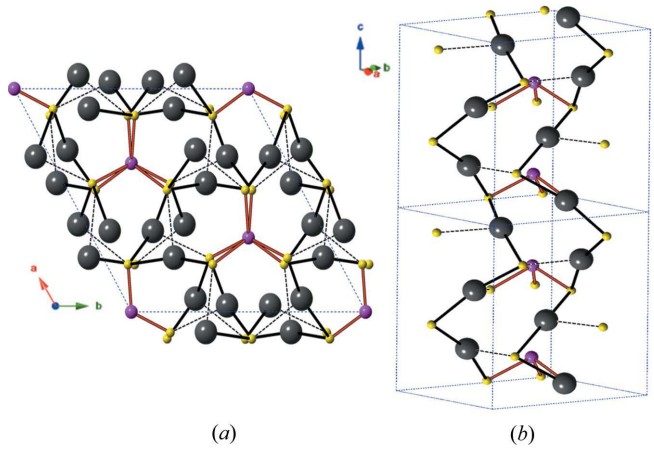

(*a*) (*b*)

Figure 6
(*a*) Crystal structure of proustite viewed along [0001]. In (*b*), the spiral of Ag—S—Ag bonds running along *c* are shown.

3.3. Polybasite isotypic series and related benleonardite and fettelite

Silver- and copper-bearing sulfosalts are usually quite difficult to describe from a structural point of view, mostly because of the difficulty in describing the Ag^+ or Cu^+ electron density. Indeed, both Ag^+ or Cu^+ d^{10} elements easily adopt various complex asymmetric coordinations due to an *s*/*d* orbital mixing and/or polarization factors (Gaudin *et al.*, 2001 and references therein). Therefore, it is common to find Ag^+ or Cu^+ in different but very close sites, which favor the presence of strong ionic conductivity. The ease to deform the electron density lowers the activation energy of the site-to-site jumps giving rise to some disorder in the crystal structure. In fast ionic conductors, also termed superionic conductors, an ionic species can move easily, giving a liquid-like structure in an open framework (tunnels, layers, *etc.*), as it was observed in the pearceite–polybasite minerals (Bindi *et al.*, 2006*a*,*b*, 2007*a*,*b*,*c*; Evain *et al.*, 2006).

The pearceite–polybasite minerals have been known for a long time and were divided by Frondel (1963) into two series: the first formed by pearceite $(Ag,Cu)_{16}(As,Sb)_2S_{11}$ and antimonpearceite $(Ag,Cu)_{16}(Sb,As)_2S_{11}$, characterized by a 'small' unit-cell [labeled 111] and high Cu content; the second formed by polybasite $(Ag,Cu)_{16}(Sb,As)_2S_{11}$ and arsenpolybasite $(Ag,Cu)_{16}(As,Sb)_2S_{11}$, with double cell parameters [labeled 222] and low Cu content. Moreover, the existence of an intermediate type of unit-cell labeled 221 was claimed for both polybasite (Harris *et al.*, 1965; Edenharter *et al.*, 1971) and arsenpolybasite (Minčeva-Stefanova *et al.*, 1979). From a crystallographic point of view these minerals were initially reported as monoclinic *C*2/*m*, although dimensionally pseudo-hexagonal (Peacock & Berry, 1947; Frondel, 1963; Harris *et al.*, 1965; Hall, 1967; Sugaki *et al.*, 1983). Bindi *et al.* (2006*a*)

recently solved and refined the crystal structure of pearceite in the space group $P\bar{3}m1$. They showed that the pearceite structure can be described as a regular alternation of two module layers stacked along the *c* axis: a first module layer (labeled *A*), with the general composition $[(Ag, Cu)_6(As, Sb)_2S_7]^{2-}$, and a second module layer (labeled *B*), with the general composition $[Ag_9CuS_4]^{2+}$. The fast ion conductivity occurs in the latter module layer (Fig. 7). Although no long range ordering at low temperature could be established for pearceite, this ordering was shown in different polybasites by Evain *et al.* (2006), who showed complex polytypism phenomena (*i.e.* 221 and 222 unit-cell types). These authors solved and refined the crystal structure of both polybasite-221 (space group *P*321) and polybasite-222 (space group *C*2/*c*) and proposed a possible mechanism regulating the ordering in these minerals. The crystal structures of the remaining members of the group (*i.e.* antimonpearceite, arsenpolybasite-221 and -222) were studied at room temperature by Bindi *et al.* (2006*b*). These authors showed that antimonpearceite possesses the same structural arrangement observed for pearceite and that the polytypism phenomena occurring in different arsenpolybasites (*i.e.* 221 and 222 unit-cell types) show strong analogies of those observed in polybasites.

It was then clear that all the members of the pearceite–polybasite group present the same high-temperature structure and is observed at room temperature either in the high-temperature fast ion conductivity form (pearceite) or in one of the low-temperature fully ordered (222), partially ordered (221) or still disordered (111) forms, with transition temperatures slightly above or below room temperature. A detailed investigation of the phase transitions, by means of conductivity and calorimetric studies and *in situ* single-crystal X-ray diffraction experiments, was carried out by Bindi *et al.* (2006*b*).

The determination of the crystal structures for all members of the group and the elucidation of all conducting mechanisms permitted us to consider these minerals as a family of polytypes. This allowed us to use only two names for all minerals of the group: pearceite or polybasite. The main reason for doubling the unit-cell parameters is linked to the ordering of silver. Given this designation, the old names antimonpearceite and arsenpolybasite were abandoned (Bindi *et al.*, 2007*b*) and the old names pearceite and polybasite, previously defined on a structural basis (*i.e.* 111 and 222), were redefined on a chemical basis.

If Ag is the main driving force responsible for the fast ionic conductivity, Cu seems to play an important role in the disorder of particular portions of the structure. Bindi *et al.* (2007*b*) showed that not all the 111 aristotype structures give a long-range ordered low-temperature structure. There are indeed Cu-poor pearceite–polybasite minerals that remain trigonal with the 111 cell and space group $P\bar{3}m1$, and intermediate pearceite–polybasite minerals with the 221 cell and space group *P*321. This particularity is related to the disorder occurring, independent of temperature, within the $[(Ag, Cu)_6(As, Sb)_2S_7]^{2-}$ *A* module layer. Indeed, with the lowest (1.54, 1.29, 1.08) and the highest (4.5) Cu content (in atoms per formula unit), Bindi *et al.* (2007*b*) obtained two different fully ordered structures. As the Cu content increases (2.29, 1.69 and 1.55) from the lowest values, 221 compounds with only a partial ordering were observed. For a further increase of Cu content (3.8), the structure remained disordered (111 cell) independent of temperature.

In conclusion, the pearceite–polybasite group of minerals can be considered as a homogeneous series with the same aristotype, fast ion-conducting form at high temperature. Depending upon the Cu content, an ordering occurs with transition temperatures related to the content: the lower the Cu content, the higher the transition temperature from the fast ion-conducting high-temperature form to the non-ion-conducting form.

Recently, Bindi *et al.* (2015*c*) showed that benleonardite, originally reported as $Ag_8(Sb, As)Te_2S_3$ by Stanley *et al.* (1986), is actually another member of the polybasite series. The benleonardite structure consists, as described above, of a stacking arrangement of $[Ag_6(Sb, As)_2S_6Te]^{2-}$ *A* and $[Ag_9Cu(S, Te)_2Te_2]^{2+}$ *B* layer modules. In the structure, two S-positions are completely replaced by Te (*i.e.* Te3 and Te4) and one exhibits the $S_{0.514\ (9)}Te_{0.486\ (9)}$ occupancy. On the basis of information gained from the structural characterization, the crystal-chemical formula of benleonardite was revised according to the structural results, yielding $Ag_{15}Cu(Sb, As)_2S_7Te_4$ ($Z = 1$) instead of $Ag_8(Sb, As)Te_2S_3$ ($Z = 2$) as previously reported.

Another interesting mineral structure, which shows similarities with those of the pearceite–polybasite minerals, is that of fettelite, $[Ag_6As_2S_7][Ag_{10}HgAs_2S_8]$. The crystal structure of fettelite (Bindi *et al.*, 2009) consists of alternating layers along the *c* axis: layer *A* with general composition $[Ag_6As_2S_7]^{2-}$ and layer *B* with general composition $[Ag_{10}HgAs_2S_8]^{2+}$. In this structure, the Ag atoms adopt various coordinations extending from quasi linear to quasi tetrahedral, the AsS_3 groups form

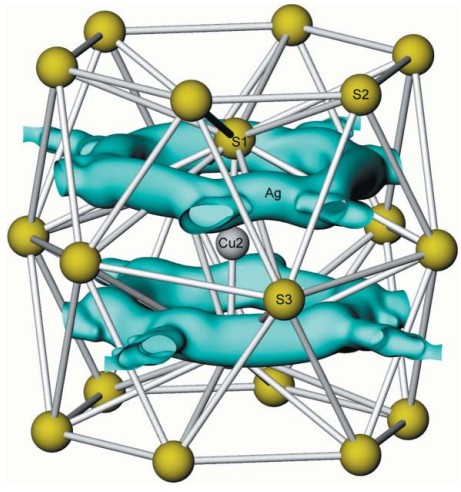

Figure 7
Non-harmonic joint probability density isosurface for Ag at room temperature in the $[Ag_9CuS_4]$ *B* layer of the pearceite structure, exhibiting silver diffusion in the *ab* plane. Level of the map: 0.05 Å^{-3}. S and Cu atoms in arbitrary size.

pyramids typically observed in sulfosalts, and Hg links two S atoms in a linear coordination. By means of an integrated high-temperature single-crystal X-ray diffraction (HT-SCXRD), differential scanning calorimetry (DSC) and complex impedance spectroscopy (CIS) study, Bindi & Menchetti (2011) showed that fettelite exhibits an ionic transition at about 107°C towards a disordered phase, having trigonal symmetry with the *a* and *b* unit-cell parameters halved. In the high-temperature structure, what induces the disorder in the *B* layer are both Ag and Hg cations, which are found in various sites corresponding to the most pronounced probability density function locations of diffusion-like paths. So, even if Hg is a minor element in fettelite, it plays an important role in the stabilization of disorder. The study by Bindi & Menchetti (2011) indicated that at least two polytypes could exist for fettelite, the ordered, monoclinic room-temperature structure (space group $C2$), and a fast ion conducting, disordered, high-temperature trigonal form (space group $P\bar{3}m1$) with *a* and *b* parameters halved.

3.4. Dervillite

Dervillite, Ag_2AsS_2, was first structurally studied by Bari *et al.* (1983) by means of X-ray single-crystal precession photographs and an X-ray powder diffraction study of the holotype. These authors found that dervillite is monoclinic with $a = 6.833$ (2), $b = 12.932$ (2), $c = 9.638$ (2) Å, $\beta = 99.33$ (2)°, $V = 1715.9$ (7) Å^3 and $Z = 8$, and crystallizes in the space group $P2/a$. In the course of a research project dealing with Ag-rich minerals from the Lengenbach quarry, Switzerland, Bindi *et al.* (2013*b*) discovered a new dervillite occurrence and were able to determine its crystal structure (Fig. 8). It crystallizes in the space group Pc, with $a = 9.6155$ (7), $b = 12.9331$ (8), $c = 6.8616$ (5) Å, $\beta = 99.352$ (8)°, $V = 842.0$ (1) Å^3 and $Z = 8$. In the crystal structure [$R_1 = 0.060$ for 2370 reflections with $I > 2\sigma(I)$], Ag adopts various coordinations extending from quasi-linear to quasi-tetrahedral whereas As forms very peculiar crystal-chemical environments, like As(S_2As) and As(S_2AsAg). Such metalloid–metalloid or metal–metalloid bonds account for the apparent charge imbalance observed in the chemical formula.

The presence of dimeric $[As_2S_4]^{4-}$ ions with a central As—As bond in dervillite could suggest a formula such as $[Ag^{+1}]_4[As_2]^{4+}[S^{2-}]_4$. However, it is difficult to analyse such polycationic compounds in strict bond-valence terms, since the electronegativity of such elements lies between that of common cations and anions. The weak Ag—As bonds in dervillite are good examples of the 'anionic' behavior, which could be explained through dative donation of the As lone pair to the closed-shell d^{10} of Ag^+ cations (Bindi *et al.*, 2013*b*).

Analogies with the dervillite structure can be found in tvalchrelidzeite, Hg_3SbAsS_3 (Yang *et al.*, 2007), pääkkonenite Sb_2AsS_2 (Bonazzi *et al.*, 1995) and chalcothallite $Tl_2(Cu,Fe)_6SbS_4$ (Makovicky *et al.*, 1980). In all of these structures, either metalloid–metalloid or metal–metalloid bonds are present, or even entire antimonide portions exist. Localized As—As bonds have been exceptionally reported in other complex sulfosalts, for example, in sterryite, $Cu(Ag,Cu)_3Pb_{19}(Sb,As)_{22}(As_2)S_{56}$ (Moëlo *et al.*, 2012).

3.5. Argyrodite–canfieldite series

The minerals of the argyrodite group cannot be classified as sulfosalts s.s. according to Moëlo *et al.* (2008). However, they are discussed for their relationships with Ag-rich sulfosalts, showing similar properties. Moreover, the occurrence of Laves polyhedra (Fig. 9*a*), similar to those described, for instance, in the crystal structures of tetrahedrite, is another particular feature (*e.g.* Makovicky *et al.*, 2005). Argyrodite Ag_8GeS_6, canfieldite Ag_8SnS_6 and putzite $(Cu_{4.7}Ag_{3.3})GeS_6$ are members of this group. According to Wang (1978), argyrodite and canfieldite are isostructural (space group $Pna2_1$ or $Pnam$), and a solid solution exists between these two minerals. The crystal structure of argyrodite has been published by Eulenberger (1977) and that of a tellurian variant of canfieldite has been reported by Bindi *et al.* (2012). Several structural studies on synthetic argyrodite-type compounds have been reported,

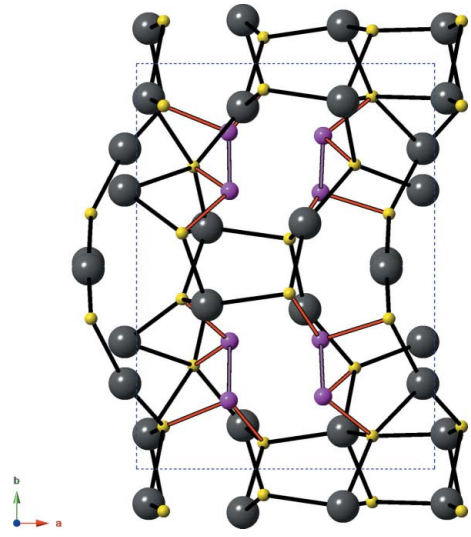

Figure 8
Projection of the crystal structure of dervillite. Thick magenta lines represent As—As bonds.

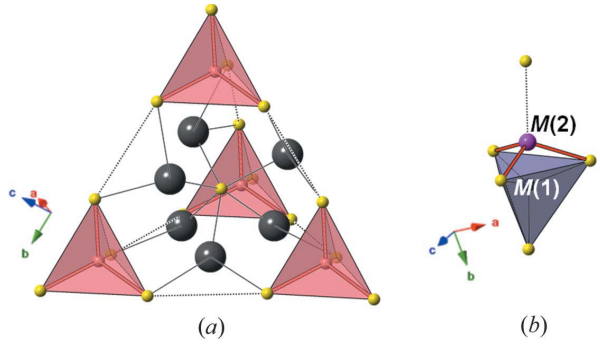

Figure 9
Structural features of members of the argyrodite group: (*a*) the Laves polyhedra in argyrodite and (*b*) the split pair of $^{M(1)}As^{5+}S_4$ and $^{M(2)}As^{3+}S_3$ sites in spryite. The vertices of the Laves polyhedra in argyrodite are completed by GeS_4 tetrahedra (in pink).

mainly because such phases are of interest for their manifold structural and physical properties, for example, as electrolytes (*e.g.* Evain *et al.*, 1998; Gaudin *et al.*, 2001; Rao & Adams, 2011). These compounds undergo three-phase transitions: the high-temperature phase crystallizes in the space group $F\bar{4}3m$. The medium-temperature phase, usually refined using a 'non-harmonic approach' (see above) has the space group $P2_13$, and, finally, the low-temperature phase has the apparent space group $F\bar{4}3m$, but actually adopts an orthorhombic symmetry (space groups: $Pna2_1$, $Pnam$ or $Pmn2_1$).

Recently Bindi *et al.* (2017*a*) reported a heretofore unobserved compound belonging to the argyrodite group, named spryite, exhibiting the ideal formula $Ag_8(As^{3+}_{0.5}As^{5+}_{0.5})S_6$, which represents the first As^{3+}-bearing member of the argyrodite group. It was found in the Ag- and Mn-rich zone of the Uchucchacua polymetallic deposit, Oyon district, Catajambo, Lima Department, Peru. From a structural point of view, spryite is intimately twinned with six twin domains. The most peculiar feature is that arsenic is present in both the trivalent and pentavalent state, occupying a split pair of sites labeled *M*(1) and *M*(2). The former has a tetrahedral coordination, typical of (As^{5+}, Ge^{4+}), whereas the latter has a trigonal pyramidal geometry characteristic of As^{3+} (Fig. 9*b*); Ag occupies sites with coordination ranging from quasi-linear to almost tetrahedral connected into a framework.

Noteworthy, a network of non-interacting Ag cations is established for spryite. This behavior is different with respect to that usually reported for argyrodite-like compounds (Belin, 2001), which show a strong disorder in the sub-lattice of the moving cations at room temperature. In this light, spryite represents the first argyrodite-type compound that does not behave as a fast ionic conductor. It is likely that the presence of As^{3+} inhibits the typical ionic conductivity observed in these compounds. The presence of partially occupied $As^{3+}S_3$ pyramids could indeed hinder the formation of the 'quasi-liquid like' structure of the mobile ions which are usually highly delocalized over the sites available to them. The free energy associated with the regular sites in spryite is likely to be higher than that of the interstitial sites, thus making the conduction mechanism highly unfavorable.

4. Conclusions

We have provided a summary of experimental studies on selected sulfides and sulfosalts where Cu and Ag play an important structural role. Our main goal was to stress the leading role of such minerals in the improvement of our knowledge about solid-state processes with possible know-how transfer to material sciences and engineering. Besides these aspects, it could be considered that in present society, a deep knowledge of (Ag, Cu)-bearing minerals is becoming increasingly important, not only because they are the source of several useful metals, but also for their interesting applications in high-tech fields.

Acknowledgements

The paper benefited from the official reviews made by Frantisek Laufek and an anonymous reviewer.

Funding information

This research received support from the University of Florence Progetto di Ateneo 2015' issued to LB and from MIUR through project SIR 2014 'THALMIGEN - Thallium: Mineralogy, Geochemistry, and Environmental Hazards', granted to CB (grant No. RBSI14A1CV).

References

Andreasen, J. W., Makovicky, E., Lebech, B. & Møller, S. K. (2008). *Phys. Chem. Miner.* **35**, 447–454.
Bari, H., Cesbron, F., Moëlo, Y., Permingeat, F., Picot, P., Pierrot, R., Schubnel, H.-J. & Weil, R. (1983). *Bull. Minéral.* **106**, 519–524.
Beland, R. (1948). *Econ. Geol.* **43**, 119–132.
Belin, R. (2001). *Solid State Ion.* **143**, 445–455.
Belov, N. V. & Pobedimskaya, E. A. (1969). *Sov. Phys. Cryst.* **13**, 843–847.
Beudant, F. S. (1832). *Traité Élémentaire de Minéralogie*, 2nd edition, pp. 445–447. Paris: Chez Verdière, Libraire-Éditeur.
Biagioni, C., Bindi, L. & Moëlo, Y. (2018). *Z. Kristallogr.* **233**, 269–277.
Biagioni, C., Bindi, L., Nestola, F., Cannon, R., Roth, P. & Raber, T. (2016). *Mineral. Mag.* **80**, 175–186.
Biagioni, C., Bindi, L. & Zaccarini, F. (2014*a*). *Can. Mineral.* **52**, 873–882.
Biagioni, C., Bonaccorsi, E., Moëlo, Y. & Orlandi, P. (2014*b*). *Period. Mineral.* **83**, 1–18.
Biagioni, C., Bonaccorsi, E., Moëlo, Y. & Orlandi, P. (2014*c*). *Eur. J. Mineral.* **26**, 163–170.
Biagioni, C., Bonaccorsi, E., Moëlo, Y., Orlandi, P., Bindi, L., D'Orazio, M. & Vezzoni, S. (2014*d*). *Mineral. Mag.* **78**, 101–117.
Bindi, L. (2008). *Acta Cryst.* C**64**, i95–i96.
Bindi, L., Biagioni, C., Raber, T., Roth, P. & Nestola, F. (2015*a*). *Mineral. Mag.* **79**, 1089–1098.
Bindi, L. & Evain, M. (2007). *Am. Mineral.* **92**, 886–891.
Bindi, L., Evain, M. & Menchetti, S. (2006*a*). *Acta Cryst.* B**62**, 212–219.
Bindi, L., Evain, M. & Menchetti, S. (2007*a*). *Can. Mineral.* **45**, 321–333.
Bindi, L., Evain, M., Pradel, A., Albert, S., Ribes, M. & Menchetti, S. (2006*b*). *Phys. Chem. Miner.* **33**, 677–690.
Bindi, L., Evain, M., Spry, P. G. & Menchetti, S. (2007*b*). *Am. Mineral.* **92**, 918–925.
Bindi, L., Evain, M., Spry, P. G., Tait, K. T. & Menchetti, S. (2007*c*). *Mineral. Mag.* **71**, 641–650.
Bindi, L., Keutsch, F. N., Francis, C. A. & Menchetti, S. (2009). *Am. Mineral.* **94**, 609–615.
Bindi, L., Keutsch, F. N., Morana, M. & Zaccarini, F. (2017*a*). *Phys. Chem. Miner.* **44**, 75–82.
Bindi, L., Makovicky, E., Nestola, F. & De Battisti, L. (2013*a*). *Can. Mineral.* **51**, 851–860.
Bindi, L. & Menchetti, S. (2011). *Am. Mineral.* **96**, 792–796.
Bindi, L., Nestola, F., De Battisti, L. & Guastoni, A. (2013*b*). *Mineral. Mag.* **77**, 3105–3112.
Bindi, L., Nestola, F., Graeser, S., Tropper, P. & Raber, T. (2015*b*). *Mineral. Mag.* **79**, 687–694.
Bindi, L., Nestola, F., Guastoni, A., Zorzi, A., Peruzzo, L. & Raber, T. (2012). *Can. Mineral.* **50**, 111–118.
Bindi, L., Petříček, V., Biagioni, C., Plášil, J. & Moëlo, Y. (2017*b*). *Acta Cryst.* B**73**, 369–376.
Bindi, L., Pratesi, G. & Spry, P. G. (2010). *Am. Mineral.* **95**, 1725–1729.

Bindi, L., Stanley, C. J. & Spry, P. G. (2015*c*). *Mineral. Mag.* **79**, 1213–1221.
Bonazzi, P., Borrini, D., Mazzi, F. & Olmi, F. (1995). *Am. Mineral.* **80**, 1054–1058.
Chetty, R., Bali, A. & Mallik, R. C. (2015). *J. Mater. Chem. C*, **3**, 12364–12378.
Dmitrieva, M. T., Yefremov, V. A. & Kovalenker, V. A. (1987). *Dokl. Acad. Sci. USSR Earth Sci. Sect.* **297**, 141–144.
Edenharter, A., Koto, K. & Nowacki, W. (1971). *Neues Jahr. Mineral. Monatsh*. **1971**, 337–341.
Edenharter, A. & Nowacki, W. (1974). *Z. Kristallogr.* **140**, 87–99.
Engel, P. & Nowacki, W. (1966). *Neues Jahrb. Mineral. Monatsh.* **1966**, 181–195.
Eulenberger, G. (1977). *Monatsh. Chem.* **108**, 901–913.
Evain, M., Bindi, L. & Menchetti, S. (2006). *Acta Cryst.* B**62**, 447–456.
Evain, M., Gaudin, E., Boucher, F., Petříček, V. & Taulelle, F. (1998). *Acta Cryst.* B**54**, 376–383.
Foit, F. F. Jr & Hughes, J. M. (2004). *Am. Mineral.* **89**, 159–163.
Frondel, C. (1963). *Am. Mineral.* **48**, 565–572.
Gabuda, S., Kozlova, S., Rizhikov, M. & Borisov, S. (2009). *J. Mol. Struct. Theoret. Chem.* **907**, 62–65.
Gaudin, E., Boucher, F. & Evain, M. (2001). *J. Solid State Chem.* **160**, 212–221.
George, L. L., Cook, N. J. & Ciobanu, C. L. (2017). *Minerals*, **7**, 17.
Glocker, E. F. (1831). *Handbuch der Mineralogie, Nürnberg*, 8th edition p. 432. Catalogue of the Royal Society of London.
Graeser, S., Schwander, H., Wulf, R. & Edenharter, A. (1995). *Schweiz. Mineral. Petrogr. Mitt.* **75**, 337–345.
Hall, H. T. (1966). PhD Thesis. Brown University, Province, USA.
Hall, H. T. (1967). *Am. Mineral.* **52**, 1311–1321.
Harker, D. (1936). *J. Chem. Phys.* **4**, 381–390.
Harris, D. C., Nuffield, E. W. & Frohberg, M. H. (1965). *Can. Mineral.* **8**, 172–184.
Hocart, R. (1937). *C. R. Acad. Sci.* **205**, 68–70.
Johan, Z., Mantienne, J. & Picot, P. (1974). *Bull. Soc. Fr. Minéral. Crist.* **97**, 48–53.
Johnson, M. L. & Burnham, C. W. (1985). *Am. Mineral.* **70**, 165–170.
Johnson, N. E., Craig, J. R. & Rimstidt, J. D. (1986). *Can. Mineral.* **24**, 385–397.
Johnson, N. E., Craig, J. R. & Rimstidt, J. D. (1988). *Am. Mineral.* **73**, 389–397.
Johnson, C. K. & Levy, H. A. (1974). *International Tables for X-ray Crystallography*, edited by J. A. Ibers and W. C. Hamilton, vol. IV, pp. 311–336. Birmingham: Kynoch Press.
Kalbskopf, R. (1972). *Tschermaks Mineral. Petrogr. Mitt.* **18**, 147–155.
Kalbskopf, R. (1974). *Tschermaks Mineral. Petrogr. Mitt.* **21**, 1–10.
Kaplunnik, L. N., Pobedimskaya, E. A. & Belov, N. V. (1980). *Dokl. Akad. Nauk SSSR*, **251**, 96–98.
Karup-Møller, S. & Makovicky, E. (1999). *Neues Jahr. Mineral. Abh.* **9**, 385–399.
Kasatkin, A. V., Nestola, F., Agakhanov, A. A., Škoda, R., Karpenko, V. Y., Tsyganko, M. V. & Plašil, J. (2018). *Minerals*, **8**, 185.
Kehoe, A. B., Temple, D. J., Watson, G. W. & Scanlon, D. O. (2013). *Phys. Chem. Chem. Phys.* **15**, 15477–15484.
Kocman, V. & Nuffield, E. W. (1973). *Acta Cryst.* B**29**, 2528–2535.
Krivovichev, S. V. & Filatov, S. K. (1999). *Am. Mineral.* **84**, 1099–1106.
Kuhs, W. F. (1992). *Acta Cryst.* A**48**, 80–98.
Lange, B., Scholz, F., Bautsch, H.-J., Damaschun, F. & Wappler, G. (1993). *Phys. Chem. Miner.* **19**, 486–491.
Laufek, F., Sejkora, J. & Dušek, M. (2010). *J. Geosci.* **55**, 161–167.
Leitl, M. (2007). PhD thesis, pp. 228. Institut für Anorganische Chemie, Universität Regensburg, Bavaria.
Leitl, M., Pfitzner, A. & Bindi, L. (2009). *Mineral. Mag.* **73**, 17–26.
Lu, X. & Morelli, D. T. (2013). *Phys. Chem. Chem. Phys.* **15**, 5762–5766.
Machatschki, F. (1928*a*). *Nor. Geol. Tidsskr.* **10**, 23–32.
Machatschki, F. (1928*b*). *Z. Kristallogr.* **68**, 204–222.
Makovicky, E. (1994). *Neues Jahrb. Mineral. Abh.* **168**, 185–212.
Makovicky, E. (2005). *Rev. Mineral. Geochem.* **57**, 403–434.
Makovicky, E. (2006). *Rev. Mineral. Geochem.* **61**, 156–185.
Makovicky, E. & Balić-Žunić, T. (1995). *Can. Mineral.* **33**, 655–663.
Makovicky, E., Forcher, K., Lottermoser, W. & Amthauer, G. (1990). *Mineral. Petrol.* **43**, 73–81.
Makovicky, E., Johan, Z. & Karup-Møller, S. (1980). *Neues Jahrb. Mineral. Abh.* **138**, 122–146.
Makovicky, E., Karanović, L., Poleti, D., Balić-Žunić, T. & Paar, W. H. (2005). *Can. Mineral.* **43**, 679–688.
Makovicky, E. & Karup-Møller, S. (2017). *Can. Mineral.* **55**, 233–244.
Makovicky, E. & Skinner, B. J. (1972). *Am. Mineral.* **57**, 824–834.
Makovicky, E. & Skinner, B. J. (1975). *Am. Mineral.* **60**, 998–1012.
Makovicky, E. & Skinner, B. J. (1979). *Can. Mineral.* **17**, 619–634.
Makovicky, E., Tippelt, G., Forcher, K., Lottermoser, W., Karup-Møller, S. & Amthauer, G. (2003). *Can. Mineral.* **41**, 1125–1134.
Makovicky, E. & Topa, D. (2014). *Mineral. Mag.* **78**, 387–414.
Marumo, F. (1967). *Z. Kristallogr.* **124**, 352–368.
Marumo, F. & Burri, G. (1965). *Chimia*, **19**, 500–501.
Marumo, F. & Nowacki, W. (1964). *Schweiz Mineral. Petrogr. Mitt.* **44**, 440–454.
Maske, S. & Skinner, B. J. (1971). *Econ. Geol.* **66**, 901–918.
Matzat, E. (1972). *Tschermaks Mineral. Petrogr. Mitt.* **18**, 312–316.
Minčeva-Stefanova, I., Bonev, I. & Punev, L. (1979). *Geokhim. Miner. Petrol.* **11**, 13–34.
Moëlo, Y., Guillot-Deudon, C., Evain, M., Orlandi, P. & Biagioni, C. (2012). *Acta Cryst.* B**68**, 480–492.
Moëlo, Y., Makovicky, E., Mozgova, N. N., Jambor, J. L., Cook, N., Pring, A., Paar, W. H., Nickel, E. H., Graeser, S., Karup-Møller, S., Balić-Žunić, T., Mumme, W. G., Vurro, F., Topa, D., Bindi, L., Bente, K. & Shimizu, M. (2008). *Eur. J. Mineral.* **20**, 7–62.
Nakai, I. & Appleman, D. E. (1983). *Am. Mineral.* **68**, 235–244.
Nasonova, D. I., Presniakov, I. A., Sobolev, A. V., Verchenko, V. Yu., Tsirlin, A. A., Wei, Z., Dikarev, E. & Shevelkov, A. V. (2016). *J. Solid State Chem.* **235**, 28–35.
Nowacki, W. (1982). *Sov. Phys. Crystallogr.* **27**, 26–27.
Nyman, H. & Hyde, B. G. (1981). *Acta Cryst.* A**37**, 11–17.
Palvadeau, P., Meerschaut, A., Orlandi, P. & Moëlo, Y. (2004). *Eur. J. Mineral.* **16**, 845–855.
Pattrick, R. A. D. & Hall, A. J. (1983). *Mineral. Mag.* **47**, 441–451.
Pauling, L. (1930). *Z. Kristallogr.* **74**, 213–225.
Pauling, L. & Neuman, E. W. (1934). *Z. Kristallogr.* **88**, 54–62.
Peacock, M. A. & Berry, L. G. (1947). *Mineral. Mag.* **28**, 2–13.
Pervukhina, N. V., Borisov, S. V., Magarill, S. A., Vasil'ev, V. I. & Kuratieva, N. V. (2010*a*). *J. Struct. Chem.* **51**, 683–688.
Pervukhina, N. V., Borisov, S. V., Magarill, S. A., Vasuliev, V. I., Kuratieva, N. V. & Kozlova, S. G. (2010*b*). *J. Struct. Chem.* **51**, 898–903.
Peterson, R. C. & Miller, I. (1986). *Mineral. Mag.* **50**, 717–721.
Pfitzner, A. (1994). *Z. Anorg. Allg. Chem.* **620**, 1992–1997.
Pfitzner, A. (1995). *Z. Anorg. Allg. Chem.* **621**, 685–688.
Pfitzner, A. (1998). *Z. Kristallogr. Cryst. Mater.* **213**, 228–236.
Pfitzner, A., Evain, M. & Petříček, V. (1997). *Acta Cryst.* B**53**, 337–345.
Pohl, D., Liessmann, W. & Okrugin, V. M. (1996). *Neues Jahrb. Mineral. Monatsh.* **1996**, 1–8.
Rao, R. P. & Adams, S. (2011). *Phys. Status Solidi A*, **208**, 1804–1807.
Ribár, B. & Nowacki, W. (1970). *Acta Cryst.* B**26**, 201–207.
Rozhdestvenskaya, I. V., Zayakina, N. V. & Samusikov, V. P. (1993). *Miner. Z.* **15**, 9–17.
Sack, R. O. & Loucks, R. R. (1985). *Am. Mineral.* **70**, 1270–1289.
Schönau, K. A. & Redfern, S. A. T. (2002). *J. Appl. Phys.* **92**, 7415–7424.
Škácha, P., Sejkora, J., Palatinus, L., Makovicky, E., Plášil, J., Macek, I. & Goliáš, V. (2016). *Mineral. Mag.* **80**, 1115–1128.
Škácha, P., Sejkora, J. & Plášil, J. (2018). *Mineral. Mag.* **82**, 199–209.

Skinner, B. J., Luce, F. D. & Makovicky, E. (1972). *Econ. Geol.* **67**, 924–938.
Spiridonov, E. M., Krapiva, L. Y., Gapeev, A. K., Stepanov, V. I., Prushinskaya, E. Y. & Volgin, V. Y. (1981). *Dokl. Akad. Nauk SSSR*, **261**, 971–976.
Stanley, C. J., Criddle, A. J. & Chisholm, J. E. (1986). *Mineral. Mag.* **50**, 681–686.
Suekuni, K., Tsuruta, K., Kunii, M., Nishiate, H., Nishibori, E., Maki, S., Ohta, M., Yamamoto, A. & Koyano, M. (2013). *J. Appl. Phys.* **113**, 043712.
Sugaki, A., Kitakaze, A. & Yoshimoto, T. (1983). *Sci. Rep. Tohoku Univ. Ser.* pp. 3 Mineralogy, Petrology and Economic Geology, **15**, 461–469.
Topa, D. & Makovicky, E. (2016). *Mineral. Mag.* **80**, 819–840.
Toulmin, P. (1963). *Am. Mineral.* **48**, 725–736.
Vasil'ev, V. I. (1968). In *Problems of the Metallogeny of Mercury*, pp. 111–129. Izdatelstvo 'Nauka' Moskva.
Vasil'ev, V. I., Pervukhina, N. V., Borisov, S. V., Magarill, S. A., Naumov, D. Yu. & Kurat'eva, N. V. (2010). *Geol. Ore Dep.* **52**, 656–661.
Wang, N. (1978). *Neues Jahrb. Mineral. Monatsh*. **1978**, 269–272.
Wei, K., Hobbis, D., Wang, H. & Nolas, G. S. (2018). *J. Electron. Mater*. **47**, 2374–2377.
Weil, R. & Hocart, R. (1953). *C. R. Congr. Natl Soc. Savantes Sect. Sci.* pp. 183–188.
Whitfield, H. J. (1980). *Solid State Commun.* **33**, 747–748.
Wuensch, B. J. (1964). *Z. Kristallogr.* **119**, 437–453.
Wuensch, B. J., Takéuchi, Y. & Nowacki, W. (1966). *Z. Kristallogr.* **123**, 1–20.
Yan, C., Gu, E., Liu, F., Lai, Y., Li, J. & Liu, Y. (2013). *Nanoscale*, **5**, 1789–1792.
Yang, H., Downs, R. T., Costin, G. & Eichler, C. M. (2007). *Can. Mineral.* **45**, 1529–1533.
Zucker, U. H. & Schulz, H. (1982). *Acta Cryst.* A**38**, 568–576.